PCCP

COMMUNICATION

View Article Online
View Journal | View Issue

Cite this: *Phys. Chem. Chem. Phys.*, 2018, **20**, 28370

Received 10th September 2018,
Accepted 30th October 2018

DOI: 10.1039/c8cp05730c

rsc.li/pccp

Patterned formation of enolate functional groups on the graphene basal plane†

Andrew Cassidy, *[a] Stine Pedersen,[a] Hendrik Bluhm,[b] Valentin Calisti,[c] Thierry Angot,[c] Eric Salomon,[c] Régis Bisson [c] and Liv Hornekær[a]

Chemical functionalization of graphene is one method pursued to engineer new properties into a graphene sheet. Graphene oxide is the most commonly used chemical derivative of graphene. Here we present experimental evidence for the formation of enolate moieties when oxygen atoms are added to the graphene basal plane. The exotic functional groups are stabilized by simultaneous bond formation between the graphene sheet and the underlying Ir(111) substrate. Scanning tunneling microscopy images demonstrate the patterned nature of C–O bond formation and X-ray photoelectron spectroscopy and high-resolution electron energy loss spectroscopy are used to characterize the enolate moiety. The results present a new mechanism for the formation of patterned graphene oxide and provide evidence of a functional group rarely considered for graphene oxide materials.

Graphene is a 2D semi-metal in which all carbon atoms are sp^2 hybridized.[1] Chemical functionalization of graphene is driven by the desire to engineer the physical and chemical properties of pristine graphene sheets, and to introduce new means of incorporating graphene interfaces with other materials.[2–4] The addition of simple atomic species, such as hydrogen,[5] oxygen[6,7] or fluorine,[8] has been shown to change the electronic band structure of graphene from that of a semi-metal to that of a semi-conductor or insulator.

Graphene oxide is a term used to describe graphene materials that have been subjected to oxidation reactions. Supported graphene oxide materials have been studied as sensor materials, for their potential magnetic properties and as clusters to form graphene oxide quantum dots.[9–12] The growth of metallic nanoparticles on supported graphene sheets is also facilitated by the presence of C–O bonds at the graphene basal plane,[4] with attachment or cleavage of particle growth initiators dependent on the nature of the C–O bond.[13] This may be a viable method for atomic layer deposition on graphene films, allowing for integration of graphene sheets in more complex electronic devices.[14] Consequently, the nature of the C–O bond formed during synthesis of graphene oxide is of general interest and importance.

It is widely assumed that an oxygen atom bonding to the basal plane of a graphene sheet is initially covalently bound through the formation of an epoxy group.[15–18] The stability of different oxygen moieties on metal-supported graphene sheets was, however, recently explored for graphene islands on Ru(0001).[19] Those authors, building on theoretical results from Jung *et al.*,[20] provided the first experimental evidence for the existence of the enolate moiety when oxygen atoms bind to a graphene sheet supported by a metal substrate. Their calculations indicate that interaction with an underlying metallic substrate can guide the formation of enolate groups when an oxygen atom binds to one carbon atom, and the adjacent carbon atom is suitably positioned to bind down to an underlying metal atom. A 370 meV gain in energy was reported for the formation of an enolate group, *versus* an epoxy group, in certain areas of the moiré pattern formed between the graphene lattice and atoms from the Ru(0001) surface.[19]

Graphene on Ru(0001), however, is already a strongly coupled system with good evidence for the preexistence of a carbon–metal bond even before oxygen atoms are introduced.[21] Hence, it is timely to consider the nature of the C–O bond for other, less strongly coupled systems. Graphene on Ir(111) (Gr/Ir(111)) demonstrates weak van der Waals interaction between the graphene sheet and the Ir(111) surface atoms.[22] Moreover, single crystal graphene sheets with a low concentration of defects and highly oriented domains are routinely prepared on Ir(111) substrates following chemical vapour deposition.[23]

The attachment of oxygen atoms to Gr/Ir(111) has been reported previously but the possibility of enolate formation was not considered.[15,16] Here, we revisit this system adding new high-resolution electron energy loss spectroscopy (HREELS) data to demonstrate that at a low flux of oxygen atoms, enolate

[a] *Department of Physics and Astronomy, Aarhus University, Denmark. E-mail: amc@phys.au.dk*
[b] *Chemical Sciences Division, Lawrence Berkeley National Lab, Berkeley, CA 94720, USA*
[c] *Aix-Marseille Univ, CNRS, PIIM, Marseille, France*

† Electronic supplementary information (ESI) available: Experimental detail, XPS fitting parameters and extra STM images. See DOI: 10.1039/c8cp05730c

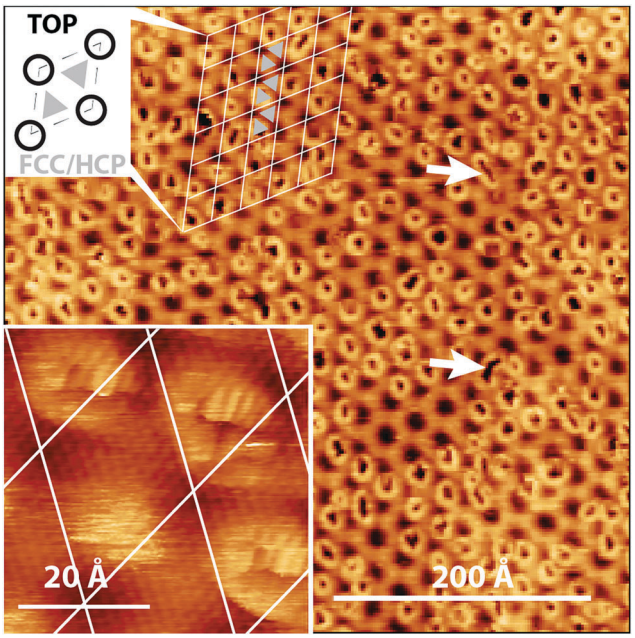

Fig. 1 Scanning tunnelling microscopy images of graphene on Ir(111) exposed to a low flux of O atoms at room temperature. The schematic and overlying lattice in the top left identify the repeating dark depressions as "TOP" regions in the moiré pattern. Newly formed C–O bonds appear throughout as circular ring features and are exclusively found at FCC and HCP regions; V = 450 mV, I = 0.20 nA. The inset shows an atomically resolved area where new C–O bonds have been formed; a moiré lattice has been superimposed; V = −16 mV, I = 0.45 nA.

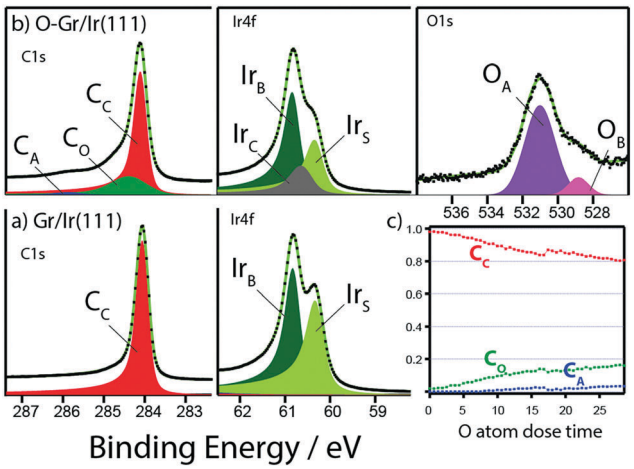

Fig. 2 X-ray photoelectron spectroscopy data for (a) pristine graphene on Ir(111) and (b) oxidized graphene on Ir(111). Individual peak details are given in Table S1 (ESI†). (c) Time evolution of the relative area of the C1s peaks with increasing fluence of O atoms.

formation dominates and occurs only at select sites on the Gr/Ir(111) surface, generating a long-range pattern of graphene oxide nano-dots.

The slight lattice mis-match between the carbon atoms in the graphene sheet and the Ir(111) surface atoms leads to a long-range repeating moiré pattern.[23] The moiré unit cell contains: TOP regions where Ir surface atoms are positioned directly beneath the center of a hexagonal ring in the graphene sheet; and HCP and FCC regions, where every second C atom is positioned directly above an Ir atom. HCP and FCC regions differ in the arrangement of Ir atoms in the second and third Ir layer. The remaining carbon atoms, in between TOP and HCP/FCC regions, show varying degrees of overlap with underlying surface Ir atoms. This repeating moiré pattern, with a 25.2 Å repeat-distance, dominates in STM imaging of the Gr/Ir(111) basal plane. Here we use an imaging mode such that TOP sites image as dark. Details on this assignment, and other experimental details, can be found in the ESI.†

When Gr/Ir(111) is exposed to a very low flux of O atoms to produce O–Gr/Ir(111) bond formation sites are imaged as doughnut-like, bright rings with a dark center, Fig. 1. In the image in Fig. 1, not all moiré sites have become oxidized with roughly one third of moiré unit cells remaining pristine. In the majority of moiré unit cells where oxidation has occurred, only the FCC site shows oxidation but in few areas, and examples are highlighted in Fig. 1, both the FCC and HCP sites show evidence for C–O bond formation. The inset shows an atomically resolved site, where O-atoms have landed on the graphene basal plane. The localized formation of C–O bonds, only at FCC and HCP sites, strongly suggests a role for the underlying Ir substrate.

In Fig. 2, X-ray photoelectron spectroscopy (XPS) data are presented for (a) Gr/Ir(111), (b) O–Gr/Ir(111), following exposure to a low flux of O atoms, and (c) the time evolution of the C1s peaks with increasing fluence of O atoms. Spectra in Fig. 2b were recorded after 50 min irradiation and represent a saturated coverage under these dosing conditions. The C1s data for Gr/Ir(111) show one peak, C_C, fit using a Doniach-Šunjić function convoluted with a Gaussian, with a binding energy of 284.04 eV. After C–O bond formation, a new peak, C_O, is introduced at 284.33 eV and the C_C peak from pristine graphene is correspondingly reduced in intensity and has shifted to 284.09 eV. The C_C binding energy shift following oxidation is likely induced by doping of the graphene sheet. There is also a contribution from a small third peak, C_A at 285.84 eV. The data are consistent with reports on graphene oxide by others.[15,16] Here, however, we show a strong preference for O addition as one unique type of C–O moiety, as represented by the C_O peak.

Photoelectrons from the Ir4f core level, from Gr/Ir(111), show two peaks at 60.80 eV and 60.29 eV, for Ir bulk and surface atoms respectively.[24] Thus the graphene sheet is not chemically interacting with the Ir surface.[15] After oxidation, a new peak, at 60.60 eV, is introduced to represent Ir surface atoms that are involved in bond formation with the overlying graphene sheet. The pristine Ir surface peak is correspondingly reduced in intensity. There is no evidence in the Ir spectrum for Ir oxide deposits originating from the thermal cracker.

After oxidation the O1s signal is fit, predominantly, with 1 Gaussian peak, O_A, with a binding energy of 531.07 eV and a second smaller peak, O_B, at 528.83 eV. O1s data for O–Ir(111) show intensity at 530 eV and the absence of such a peak in the O–Gr/Ir(111) data illustrates that no Ir–O bond is formed.[24] Fig. 2c shows the evolution of the relative areas for the C1s peaks, with increasing fluence of O atoms. After 30 min dosing

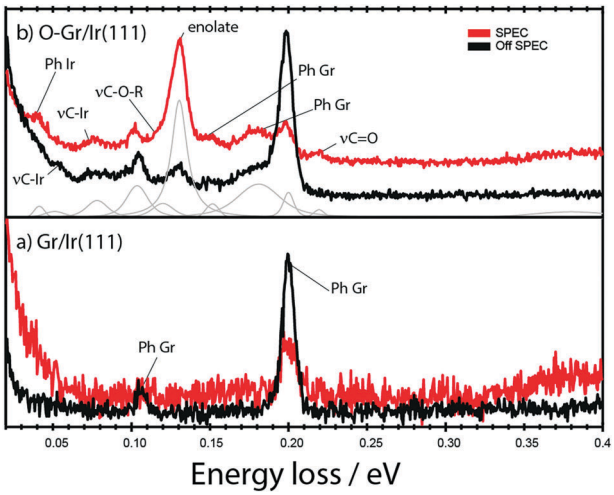

Fig. 3 High-resolution electron energy loss spectroscopy data recorded (a) on pristine graphene on Ir(111) and (b) on graphene on Ir(111) exposed to a low flux of O atoms. In both cases curves are shown for data collected in the specular and out of specular directions following irradiation with a 20 eV electron beam. The curves have been normalized to the intensity of the elastic peak. See Table 1 for peak identifications.

the coverage approximates saturation with an upper limit contribution from the C_O peak at 17% and an upper limit 3% contribution from C_A. We propose that the C_O peak corresponds both to carbon atoms bound to O-atoms, *via* formation of an enolate, and to neighbouring carbon atoms simultaneously bound to the underlying Ir substrate.[5] These percentages concur with analysis of STM images for surface coverage (S1). The size of such a cluster corresponds to the size of the FCC site in the moiré unit cell. This confirms that the most reactive sites for O atom addition are confined to the FCC region of the moiré. Experiments and DFT calculations illustrate that the position of an Ir atom directly beneath a carbon atom, and C–Ir bond formation, significantly increases the energy gain for C–H bond formation in FCC and HCP regions compared to similar bond formation in TOP regions, with a slight energetic preference for FCC regions.[5] Jung *et al.* and Novotny *et al.*, concluded that the same mechanism leads to the stabilization of enolate formation upon formation of C–O bonds for Gr/Cu, Gr/Ni and Gr/Ru.[19,20] Novotny *et al.* demonstrated that enolate formation was favoured in FCC regions of the graphene Ru(0001) moiré.

We suggest that the C_A peak is caused by either a small amount of epoxy group formation[15,16] or carbonyl formation, which we justify using HREELS data.

HREELS data, are shown in Fig. 3. The spectrum for Gr/Ir(111) shows two distinct energy loss peaks; at 104 meV for losses incurred by scattering from the ZO phonons in graphene and a second peak at 199 meV, corresponding to scattering from the LO/TO phonons.[28] After oxidation a new set of peaks is introduced, Fig. 3b. We interpret this spectrum in Table 1, in light of HREELS for H–Gr/Ir(111) reported by Kyhl *et al.*[25] and the calculated vibrations of the enolate group reported by Jung *et al.*[20]

The LO/TO and ZO phonons modes for graphene persist and in addition signals arise from scattering loses associated with: the vibration of the newly formed C–Ir bonds, reported in relation to Fig. 2, at 61 meV and 78 meV; LO/TO and ZO phonons associated with the newly formed graphane-like clusters reported in relation to Fig. 1 at 152 meV and 181 meV respectively. Three peaks, at 120 meV, 130 meV and 219 meV, can be associated with vibration of the newly formed C–O bonds and the intensity of these peaks varies with the angle at which scattered electrons are detected. In particular the peak at 130 meV is prominent in the specular direction but reduced in out-of-specular directions, indicating formation of a very polar bond.

Where available, experimental reports on the characterization of oxidized carbon substrates by HREELS are listed in Table 1.[26,27,29] There is consensus that the energy loss peak at 219 meV can be associated with vibration of a C=O bond indicating that we have formation of carbonyl species. The corresponding small HREELS intensity explains the origin of the smaller peak O_B, at 528.83 eV and C_A at 285.84 eV in XPS data discussed in Fig. 2. Energy losses at 120–135 meV have consistently been associated with vibrations from ether and epoxy groups but the strong polar nature of the peak at 130 meV observed here, and the simultaneous formation of the C–Ir

Table 1 Vibrational features in HREELS data

Vibration mode	O–Gr/Ir(111) (meV)	O–Gr/Cu(111) (meV)[20]	H–Gr/Ir(111) (meV)[25]	Oxidized diamond films
Phonon Ir	41		40	
νC–Ir	61		52	
νC–Ir	78		72	
ZO graphene	104		100	100(ν(C=C))[b 26]
ν(C–O–C) epoxy	120			57,[26] 125,[27] 135,[27] 140[c 26]
Enolate	130	28, 29, 54, 125, 145[a]		
LO/TO phonons in graphane-like clusters	152		158	
ZO phonons in graphane-like clusters	181		178	
TO/LO graphene	199		195	200–205(ν(C=C))[b 27]
ν(C=O) carbonyl	219			220,[26] 220[27]

[a] Jung *et al.* calculated 6 vibrational modes for enolate groups at two distinct sites for free standing graphene, HOPG, Gr/Cu(111) and Gr/Ni(111) substrates. The values for O–Gr/Cu(111) are included here. [b] The ν(C=C) stretching vibration does not originate from phonons as in graphene but appears with similar energy losses. [c] The region between 120–140 meV is complex for oxidized nano-diamond films and peaks assigned to ν(C–O–O–C), $\delta(CH_3)$, δ(HC=CH), aromatic δ(ring-H) and ν(C–O–H) in the literature overlap with the clear peak at 130 meV identified in Fig. 3.

bond, points to the identification of an enolate group. The vibrational energies for the 6 vibrational modes of the enolate moiety calculated by Jung *et al.* are consistent with this assignment.[20] Jung *et al.* report a substrate dependent vibration between 25–29 meV that is likely hidden by the elastic peak in Fig. 3b. The vibration at 49–58 meV for collective motions of the entire CO group normal to the graphene plane overlaps with νC–Ir, reported by Kyhl *et al.*[25]

We have demonstrated that O atoms covalently bind to the graphene basal plane selectively at sites dictated by the underlying Ir(111) substrate. The spectroscopic evidence supports the view that these new bonds take the form of enolates and microscopy demonstrates the patterned nature of bond formation. Future work will focus on exploiting the potential of using this new functional group to perform further chemistry at the graphene basal plane, and to engineer interfaces with other materials.

Conflicts of interest

There are no conflicts to declare.

Acknowledgements

We acknowledge financial support from The Danish Council for Independent Research (grant no. 5137-00049B), Innovation Fund Denmark (NIAGRA) (grant no. 5184-00018B), The European Research Council (CoG GRANN, grant no. 648551), and VILLUM FONDEN *via* the Centre of Excellence for Dirac Materials (grant no. 11744). Affiliation with the Center for Integrated Materials Research (iMAT) at Aarhus University is gratefully acknowledged. We thank The Advanced Light Source, which is supported by the Director, Office of Science, Office of Basic Energy Sciences of the U.S. Department of Energy at LBNL under contract no. DE-AC02-05CH11231.

References

1 K. S. Novoselov, A. K. Geim, S. V. Morozov, D. Jiang, Y. Zhang, S. V. Dubonos, I. V. Grigorieva and A. A. Firsov, Electric field effect in atomically thin carbon films, *Science*, 2004, **306**, 666–669.

2 N. M. Bardhan, P. V. Kumar, Z. Li, H. L. Ploegh, J. C. Grossman, A. M. Belcher and G. Y. Chen, Enhanced Cell Capture on Functionalized Graphene Oxide Nanosheets through Oxygen Clustering, *ACS Nano*, 2017, **11**, 1548–1558.

3 J. E. Johns and M. C. Hersam, Atomic covalent functionalization of graphene, *Acc. Chem. Res.*, 2013, **46**, 77–86.

4 J. E. Johns, J. M. P. Alaboson, S. Patwardhan, C. R. Ryder, G. C. Schatz and M. C. Hersam, Metal oxide nanoparticle growth on graphene via chemical activation with atomic oxygen, *J. Am. Chem. Soc.*, 2013, **135**, 18121–18125.

5 J. H. Jørgensen, A. G. Čabo, R. Balog, L. Kyhl, M. N. Groves, A. M. Cassidy, A. Bruix, M. Bianchi, M. Dendzik, M. A. Arman, L. Lammich, J. I. Pascual, J. Knudsen, B. Hammer, P. Hofmann and L. Hornekaer, Symmetry-Driven Band Gap Engineering in Hydrogen Functionalized Graphene, *ACS Nano*, 2016, **10**, 10798–10807.

6 B. Huang, H. Xiang, Q. Xu and S. H. Wei, Overcoming the phase inhomogeneity in chemically functionalized graphene: the case of graphene oxides, *Phys. Rev. Lett.*, 2013, **110**, 1–5.

7 K. Schulte, N. a. Vinogradov, M. L. Ng, N. Mårtensson and A. B. Preobrajenski, Bandgap formation in graphene on Ir(111) through oxidation, *Appl. Surf. Sci.*, 2012, **267**, 74–76.

8 M. Chen, H. Zhou, C. Qiu, H. Yang, F. Yu and L. Sun, Layer-dependent fluorination and doping of graphene via plasma treatment, *Nanotechnology*, 2012, **23**, 115706.

9 Y. Wen, C. L. Yen, L. Yan, H. Kono, S. H. Lin and Y. C. Ling, Magnetism-tuning strategies for graphene oxide based on magnetic oligoacene oxide patches model, *Phys. Chem. Chem. Phys.*, 2018, **20**, 3678–3686.

10 W. Xie, L.-T. Weng, C.-K. Chan, K. L. Yeung and C.-M. Chan, Reactions of SO_2 and NH_3 with epoxy groups on the surface of graphite oxide powder, *Phys. Chem. Chem. Phys.*, 2018, **20**, 6431–6439.

11 Y. Zhang, C. Yang, D. Yang, Z. Shao, Y. Hu, J. Chen, L. Yuwen, L. Weng, Z. Luo and L. Wang, Reduction of graphene oxide quantum dots to enhance the yield of reactive oxygen species for photodynamic therapy, *Phys. Chem. Chem. Phys.*, 2018, **20**, 17262–17267.

12 N. M. Bardhan, P. V. Kumar, Z. Li, H. L. Ploegh, J. C. Grossman, A. M. Belcher and G. Y. Chen, Enhanced Cell Capture on Functionalized Graphene Oxide Nanosheets through Oxygen Clustering, *ACS Nano*, 2017, **11**, 1548–1558.

13 C. J. Tainter and G. C. Schatz, Reactive Force Field Modeling of Zinc Oxide Nanoparticle Formation, *J. Phys. Chem. C*, 2016, **120**, 2950–2961.

14 R. H. J. Vervuurt, W. M. M. E. Kessels and A. A. Bol, Atomic Layer Deposition for Graphene Device Integration, *Adv. Mater. Interfaces*, 2017, **1700232**, 1700232.

15 R. Larciprete, S. Fabris, T. Sun, P. Lacovig, A. Baraldi and S. Lizzit, Dual path mechanism in the thermal reduction of graphene oxide, *J. Am. Chem. Soc.*, 2011, **133**, 17315–17321.

16 N. A. Vinogradov, K. Schulte, M. L. Ng, A. Mikkelsen, E. Lundgren, N. Mårtensson and A. B. Preobrajenski, Impact of atomic oxygen on the structure of graphene formed on Ir(111) and Pt(111), *J. Phys. Chem. C*, 2011, **115**, 9568–9577.

17 M. Z. Hossain, J. E. Johns, K. H. Bevan, H. J. Karmel, Y. T. Liang, S. Yoshimoto, K. Mukai, T. Koitaya, J. Yoshinobu, M. Kawai, A. M. Lear, L. L. Kesmodel, S. L. Tait and M. C. Hersam, Chemically homogeneous and thermally reversible oxidation of epitaxial graphene, *Nat. Chem.*, 2012, **4**, 305–309.

18 S. Katano, T. Wei, T. Sasajima, R. Kasama and Y. Uehara, Localized electronic structures of graphene oxide studied using scanning tunneling microscopy and spectroscopy, *Phys. Chem. Chem. Phys.*, 2018, **20**, 17977–17982.

19 Z. Novotny, M.-T. Nguyen, F. P. Netzer, V.-A. Glezakou, R. Rousseau and Z. Dohnálek, Formation of Supported Graphene Oxide: Evidence for Enolate Species, *J. Am. Chem. Soc.*, 2018, **140**, 5102–5109.

20 J. Jung, H. Lim, J. Oh and Y. Kim, Functionalization of Graphene Grown on Metal Substrate with Atomic Oxygen: Enolate vs Epoxide, *J. Am. Chem. Soc.*, 2014, **136**, 8528–8531.

21 D. Martoccia, P. R. Willmott, T. Brugger, M. Björck, S. Günther, C. M. Schlepütz, A. Cervellino, S. A. Pauli, B. D. Patterson, S. Marchini, J. Wintterlin, W. Moritz and T. Greber, Graphene on Ru(0001): A 25 × 25 supercell, *Phys. Rev. Lett.*, 2008, **101**, 1–4.

22 R. Brako, D. Šokčević, P. Lazić and N. Atodiresei, Graphene on the Ir(111) surface: From van der Waals to strong bonding, *New J. Phys.*, 2010, **12**, 113016.

23 A. T. N'Diaye, J. Coraux, T. N. Plasa, C. Busse and T. Michely, Structure of epitaxial graphene on Ir(111), *New J. Phys.*, 2008, **10**, 043033.

24 M. Bianchi, D. Cassese, A. Cavallin, R. Comin, F. Orlando, L. Postregna, E. Golfetto, S. Lizzit and A. Baraldi, Surface core level shifts of clean and oxygen covered Ir(111), *New J. Phys.*, 2009, **11**, 063002.

25 L. Kyhl, R. Balog, T. Angot, L. Hornekær and R. Bisson, Hydrogenated graphene on Ir(111): a high-resolution electron energy loss spectroscopy study of the vibrational spectrum, *Phys. Rev. B*, 2016, **93**, 115403.

26 S. Ghodbane, T. Haensel, Y. Coffinier, S. Szunerits, R. Boukherroub, S. I. U. Ahmed, J. A. Schaefer, D. Steinm, F. D. C. Gmbh, I. D. R. Interdisciplinaire, D. N. Iemn, D. Steinmüller-Nethl, R. Boukherroub, S. I. U. Ahmed and J. A. Schaefer, HREELS investigation of the surfaces of nanocrystalline diamond films oxidized by different processes, *Langmuir*, 2010, **26**, 18798–18805.

27 Z. Shpilman, I. Gouzman, E. Grossman, R. Akhvlediani and A. Hoffman, Oxidation of diamond films by atomic oxygen: High resolution electron energy loss spectroscopy studies, *J. Appl. Phys.*, 2007, **102**, 114914.

28 M. Endlich, A. Molina-Sánchez, L. Wirtz and J. Kröger, Screening of electron-phonon coupling in graphene on Ir(111), *Phys. Rev. B: Condens. Matter Mater. Phys.*, 2013, **88**, 1–4.

29 M. Acik, G. Lee, C. Mattevi, A. Pirkle, R. M. Wallace, M. Chhowalla, K. Cho and Y. Chabal, The Role of Oxygen during Thermal Reduction of Graphene Oxide Studied by Infrared Absorption Spectroscopy, *J. Phys. Chem. C*, 2011, **115**, 19761–19781.